2023

Synergetic pyrolysis of LiNi1/3Co1/3Mn1/3O2 and PET plastics shed light on highly efficient and energy saving strategies for battery recovery and regeneration

Xiaoying Lu
Faculty of Science and Technology, Technological and Higher Education Institute of Hong Kong,
xylu@thei.edu.hk

Kehua Wu
Faculty of Science and Technology, Technological and Higher Education Institute of Hong Kong

NOTIFICATION OF ACCEPTANCE

Chiba, Japan, April 7-10, 2023

http://www.icmda.org/

Name LU Xiaoying, ZHANG Zheming, BIAN Haidong and Wu Kehua

Institution 1.4)Technolgical and Higher Education Institute of Hong Kong, Hong Kong; 2,3)Shenzhen Automotive Research Institute, Beijing Institute of Technology

Email : xylu@thei.edu.hk; zhangzheming@szari.ac.cn

Abstract ID : MT23-428-A

Title : Recovery of catalysis active products from spent battery cathode materials

Dear: LU Xiaoying, ZHANG Zheming, BIAN Haidong and Wu Kehua

Thank you for your attention and support to 2023 6th International Conference on Materials Design and Applications (ICMDA 2023), which will be held in Chiba University, Japan during April 7-10, 2023. ICMDA 2023 review procedure has finished now.

We are pleased to inform you that your abstract identified above has been accepted and can be arranged as an **oral presentation** according to the comments and recommendations from reviewers and conference technical committee. You are sincerely invited to present your work and communicate with other distinguished participants at the conference.

Again, congratulations. We look forward to seeing you in Japan.

Yours sincerely,

ICMDA 2023 Organizing Committee

↓ Registration Guideline

Before finish the following registration process, please kindly noting:

Your final abstract is well reformatted according to the template.

Template

And then, please finish the following registration process:

1. The link for registration: https:/confsys.iconf.org/register/icmda2023
2. Complete all the information required on the first page. → Click “Submit”
3. Check all the information is correct and upload **your photo** and **final abstract** (.pdf).
4. Click “Submit” and choose the payment method in the next page.

   For Online Payment: You can pay the registration fee directly.

   For Bank Transfer: Please upload the payment voucher

5. Conference staff will contact you after they saw your registration record. If you don’t receive any reply from conference staff, you could send an email to the conference email box: icmda@cbees.net.
6. If you have any problem about the registration, please contact conference staff by email: icmda@cbees.net.
7. Please complete your registration Before **Feb. 15**, 2023.
8. If any questions, please feel free to contact us via icmda@cbees.net.
9. More information about the conference, please check the website www.icmda.org.

↓ Notice

Refund/Cancellation Policy

If a registrant is unable to attend the event for any reason, the conference committee encourages you to send a substitute in your place, someone who is one of the co-authors or from the same institute/organization.

Written requests for cancellations must be sent to the Conference Secretary 2 months before the event, 30 USD processing fee is required. Cancellations received less than 2 months before the event, will NOT be dismissed and registration fees will not be refund.

Personal Reason

The conference cannot refund or pay any compensation when the registrant could not attend the conference for reason of circumstances which amount to “personal reason”. Such as travel difficulties, visa problems, health issues, financial default etc.

Force Majeure

The conference cannot accept responsibility, refund or pay any compensation where the performance of the conference is prevented or affected by reason of circumstances which amount to “force majeure”.

Circumstances amounting to “force majeure” include any event which we could not, even with all due care, foresee or avoid. Such circumstances include the fire, flood, explosion, storm or other weather damage, break-in, criminal damage, riots or civil strife, industrial action, natural or nuclear disaster, fire, adverse weather conditions, war or threat of war, actual or threatened terrorist activity, epidemic and all similar situations beyond our control.

Conference Date and Place Statement

The organizer has the right to change the date and place of the conference under the reason of amount to “force majeure” circumstances. The participants of the conference are obliged to cooperate with the organizer's change and refund policy.

Synergetic pyrolysis of $LiNi_{1/3}Co_{1/3}Mn_{1/3}O_2$ and PET plastics shed light on highly efficient and energy saving strategies for battery recovery and regeneration

Abstract

With the increasing consumption of lithium-ion batteries (LIBs), it is highly desirable to develop efficient and energy saving strategies for battery material recovery and regeneration. In this study, a synergetic pyrolysis strategy was developed to recover valuable metals by thermal treatment of $LiNi_{1/3}Co_{1/3}Mn_{1/3}O_2$ (NCM) cathode materials with the addition of polyethylene terephthalate (PET) plastics. It is the first time that PET plastics served as reaction additives to accelerate the lattice decay and thermal decomposition of NCM materials. With the assistance of PET synergetic pyrolysis, NCM started to decompose at only 400°C, and was completely converted to Li_2CO_3, MnO and Ni-Co alloy after thermal reaction at 550°C for 30 min with the NCM:PET mass ratio of 1.0:0.3. The thermal degradation of PET was retarded with various free radicals and reductive gases released. Furthermore, a density functional theory (DFT) calculation verified the combination preference of O-Li bonding between horizontal PET and the Li terminated NCM (001) surface. The surface adsorption caused atom capture and the free radical/gaseous reduction reactions explained the synergetic effect of PET on promoting the lattice destruction of NCM cathode materials. Moreover, the complete decomposition of NCM well benefited the post treatment, and the subsequent

separation of Li and transition metals (TM: Ni, Co and Mn) could be efficiently achieved by water washing method. Regenerated NCM was also synthesized by using the recovered Li- and TM- containing products as feedstocks. As a result, this study provided a novel NCM recovery strategy with significant privileges of chemical free, energy saving, highly efficient and scalable. Meanwhile, this strategy proposed an ideal solution for the minimization and utilization of PET plastics. In addition, the mechanism study provided a theoretical guidance on the industrialization and broaden application of PET plastic for effective metal recovery from spent LIBs by this synergetic pyrolysis strategy.

Introduction

To meet the global requirement of energy supply and reduction in greenhouse gas emission, the market of electric vehicles has been developing and increasing rapidly over the years and is anticipated to exceed 300 million in 2030[1,2]. The lithium-ion batteries (LIBs), especially with the $LiNi_xCo_yMn_zO_2$ (x+y+z = 1, NCM) cathode materials, have been intensively investigated for electrochemical energy storage, owing to high energy density, high cell voltage, and high reliability, etc., thus serving as the leading battery packs for electric vehicle applications[3,4,5]. It is predicted that the global market for NCM cathode materials could reach US 46.4$ billion by 2027[6]. However, the exploding market of LIBs is translating into tremendous number of discarded ones, due to the limited service life time[2]. In addition to the challenge of waste storage, spent

LIBs contain hazardous materials like heavy metals (e.g. Ni and Co) and toxic electrolytes which are extremely harmful to both environment and human health. In the meantime, the metal elements in cathode materials, including Li, Ni, Co and Mn, are of high value while facing severe problems of resource depletion[7]. Thus, it is of significant implication for both environment and economy to search for an environmentally friendly metal recycling strategy from NCM cathode materials in spent LIBs.

With the advantages of large treatment capacity and simple operation procedures, pyrometallurgical treatments have already gained considerable attention with continuous research efforts in the field of metal recovery from the spent LIBs. Aided by chemical reactions under elevated temperatures, pyrometallurgy treatment can destruct the lithiated metal oxides and separate them into metal fractions that can be reclaimed via simple post treatments. Traditional pyrometallurgy, which has been widely adopted in many countries, always transforms the waste battery strips into metal alloys at high temperatures[3,8,9,10]. However, the high energy consumption hinders economic interests, and the inevitable loss of lithium during pyrolysis process remains a technical hurdle as well. To reduce treatment cost and enhance metal recovery, extensive studies have been conducted with participation of chemicals during thermal treatments, including gas, salt and other reducing agents. Chlorination or sulfation salts and mineral acids have been added to the roasting process and could convert Li into soluble LiCl or Li_2SO_4 [11,12,13,14]. For example, NCM was successfully decomposed into Li and transition metal (TM) salts after 750°C-calcination with 100 wt% Na_2SO_4 addition[15]. Although the reaction temperature can be reduced by studies above via

transferring reaction pathways, the consumption of salts or acids is high and even up to twice of spent cathode materials in mass, causing subsequent problems of waste salts and gaseous exhausts. Therefore, some other studies have paid attention on carbon-containing reductants as the cleanest reducing agents, e.g., lignite, graphite, etc.[16,17]. LCO/NCM can be decomposed and reduced to a low valence stage (Li_2CO_3, transition metal elements and oxides) without the use of inorganic acid during the thermal treatment. For example[18], previous work reported the destruction and collapse of oxygen octahedrons of NCM at around 750°C, and the reaction processes were controllable by governing the amount of additives. However, the recovery rate of each metal elements varied a lot from 81% to 100%, implying that a further decrease in reaction temperatures was expected to enhance its economic feasibility[1,3,19,20]. Thus, it still remains an urgent need and key issue to develop a chemical-free recycling strategy that is more energy-saving and efficient.

As one of the most consumed polymer resins, polyethylene terephthalate (PET) is widely applied in various fields like packaging, drinking bottles, and construction industries, thus contributing to a tremendous volume of PET production and waste generation. The most current statistics reported that the global market volume of PET reached nearly 23.7 million metric tons in 2020 and was expected to grow to 29.7 million metric tons by 2026. However, the majority of PET ended up as solid wastes[21], causing serious environmental concerns to the ocean, soil, organisms and human beings. The pyrolysis of plastic wastes, including PET, has been widely studied, as it can

effectively utilize the plastic wastes as fuel sources and reduce the waste volume at the same time. During PET pyrolysis, the oxygenated functional groups break and escape from the polymer chain. As a result, the PET was quickly decomposed at over 400°C, generating large amounts of free radicals and gases for secondary reactions[22,23,24]. Previous studies have reported that the PET co-pyrolyzation reduced the pyrolysis temperature of HDPE and altered the product compositions[24,25]. Based on the aforementioned pyrolysis properties and performance of the PET, an novel battery material recovery strategy can be expected by addition of PET plastics to the pyrolysis reactions of the NCM cathode materials. It is hypothesized that PET and its intermediate pyrolysis products could react with and deconstruct the crystal lattice of NCM materials, therefore converting target metals into separated and easy-collected phases. The proposed strategy might provide a technical solution for resource utilization of spent NCM and waste PET plastics at the same time, and simultaneously reduce energy consumption because of the synergy effects. Only C, H, O are introduced into the reaction system, without the use and production of inorganic chemicals, which can make the reaction process environmentally friendly.

Besides reaction feasibility, the reaction mechanisms should be intensively explicated to provide theoretical basis for scale-up and migration application on metal recovery industries. In recent years, density functional theory (DFT) has become the most popular theoretical framework for studying surface electron structure of battery materials[26]. By means of DFT, the (001) surface of layered $LiCoO_2$ (LCO) was reported

to have relative lower surface energy, compared with other surfaces of LCO. Thus, (001) surface was proven stable in LCO crystal strucutre[27,28]. Previous work optimized the adsorption structure of LCO and sulfur species, proving that the LCO-S(IV) anchor played a vital role in the reaction progresses. Therefore, it can be anticipated that the DFT calculation can aid in optimizing the adsorption configuration and adsorption energy between PET and NCM, which may further provide the combination preference at atomic level. In addition, the mass spectra (MS) and Fourier transform infrared spectrometer (FT-IR) coupled with thermal gravimetric analyzer (TGA) has been widely used in plastic pyrolysis studies[29] which revealed the synergy effect by monitoring the pyrolysis behaviors via TGA-MS-FTIR and comparing the blended systems with the pure materials.

Therefore, this study proposed a novel NCM-PET synergetic pyrolysis strategy to recycle valuable metals in NCM cathode materials, with the addition of PET plastics as chemical additives. The effect of pyrolysis parameters on reaction processes was comprehensively explored and the pyrolysis conditions were optimized as well. The recovery process was developed, including water washing after synergetic pyrolysis, filtration, and evaporation, which was totally chemical free. After metal recovery, new NCM materials were regenerated by employing the recovery products as reaction feedstocks. Finally, we deeply discussed the mechanisms of synergetic pyrolysis by integrating both experimental characterization and DFT theoretical calculation. The mechanism study provided theoretical verification and guidance for future scale-up and

migration applications. The proposed strategy in this study aimed at providing a “waste to resources ” solution for both PET and NCM wastes that possessed superior economic and environmental benefits.

Results

Decomposition behavior of NCM via synergetic pyrolysis

As shown in Fig 1a, the synergetic pyrolysis of NCM could be regarded as a stepwise reduction and decomposition along with the elevated temperatures. Peaks of NCM, as the primary crystal phase, were found declining slightly after 400°C pyrolysis. Meanwhile, three lithium manganese oxides ($Li_{0.5}MnO_2$, Li_3MnO_4, $LiMnO_4$) were observed with tiny peaks, which were attributed to the reconstruction of Li and TM atoms under the pyrolysis condition. The partial destruction of the NCM crystals could lead to the formation of new crystal phases. When temperature was increased to 500°C, the peaks of NCM cannot be observed and the three lithium manganese oxides still existed without obvious changes in peak intensity. Moreover, the peaks of Li_2CO_3, $NiMnO_3$, $Ni_xCo_{1-x}O$, and Ni_xCo_{1-x} were identified, indicating that some of the Ni and Co were partially reduced from trivalent to divalent ($Ni_xCo_{1-x}O$) and zero valent (Ni_xCo_{1-x}). When the temperature was further elevated to 550°C, three lithium manganese oxides and $NiMnO_3$ were eliminated and replaced with Li_2CO_3 peaks. When the pyrolysis temperature reached 600°C, NCM was fully decomposed to Li_2CO_3,

MnO and Ni_xCo_{1-x}, while the peaks of $Ni_xCo_{1-x}O$ were not detectable. The types of crystal phases remained unchanged with further treatment from 700 to 800°C, but peak intensities due to increasing crystallization of Li_2CO_3, MnO and Ni_xCo_{1-x} were clearly observed. When the temperature reached 900°C, Li_2CO_3 suddenly disappeared while LiC was observed with low peak intensity. This was possibly due to the decomposition and carbonization of Li_2CO_3. In addition, the peaks of MnO and Ni_xCo_{1-x} remained unchanged, when compared with the XRD patterns of samples pyrolyzed at 800°C. When the sample was pyrolyzed at 1000°C, it is interesting that LiC, Mn_xNi_{1-x} and Mn_xCo_{1-x} were found in the XRD patterns, thus illustrating that the TM (Ni, Co and Mn) were finally reduced to zero valence with the formation of solid solutions. The phase transformation of Ni, Co and Mn represented a gradual reduction of Mn(IV), Ni(II) and Co(III) to Mn (0), Ni (0) and Co (0), respectively.

Furthermore, Fig 1b revealed the effect of NCM/PET mass ratio on the reaction series under 600°C pyrolysis. When a small amount of PET was mixed with NCM (NCM:PET mass ratio of 1.0:0.1), NCM was not fully decomposed with a remaining peak at 18.7°. Meanwhile, Li_2CO_3, $Ni_xCo_{1-x}O$ and Ni_xCo_{1-x} were observed as the product phases, due to the thermal decomposition of NCM. When the NCM:PET ratio was changed to 10:0.2, the crystal phase of NCM was completely diminished with the peaks of Ni_xCo_{1-x} and MnO growing but $Ni_xCo_{1-x}O$ decreasing. When the NCM:PET ratio was varied to 10:0.3, the disappearance of $Ni_{1-x}Co_{1-x}O$ was found, probably due to its reduction to zero-valent metals. Interestingly, extra PET addition (NCM:PET=1.0:1.0) showed no

influence on the phase composition and peak intensity of the products. To investigate the effect of PET addition on crystal phase change in the reaction system, pure NCM was also pyrolyzed under nitrogen atmosphere and the corresponding XRD pattern was given in Fig. S1 of Supporting Information (SI). It is revealed that no crystal phase transformation occurred for the pure NCM sample, even elevated to 600°C. Therefore, the comparison implied that PET played a pivotal role in the decomposition of NCM sample. PET (or its pyrolysis products) could stimulate the structure collapse of NCM for efficient separation of Li and TM, and simultaneously possess reducibility to transform Ni/Co(II) into alloys. The effect of pyrolysis duration time on crystal phase change was further presented in Fig. 1c. It is obvious that the majority of NCM was quickly decomposed into Li_2CO_3, $Ni_xCo_{1-x}O$, Ni_xCo_{1-x} and MnO within only 15 min. After 30 min, the peaks of NCM fully disappeared and the $Ni_xCo_{1-x}O$ phase also vanished, and meanwhile, the peaks of Ni_xCo_{1-x} were heightened, owing to continuous reduction of Ni and Co. With the increase of pyrolysis temperature from 60 min to 120 min, no obvious change in XRD patterns for the pyrolyzed products, thus implying that the phase transformation terminated within 30 min. To demonstrate the effectiveness of NCM-PET synergetic pyrolysis strategy, the metal recovery rate was calculated for the pyrolyzed products under different temperatures (Fig. 2). The element Li, Ni, Co and Mn were about 100% remained in the solid phase products, given that the pyrolysis temperature was no higher than 700°C. With the further increase of pyrolysis temperatures, the Li was lost by 4% at 800°C, while the recovery rate of Ni, Co and Mn was dropped by 5-7% at 900°C. Therefore, to minimize energy and chemical

consumption and simplify product speciation, the optimal parameters for the synergetic pyrolysis were set as 600°C, 30 min and NCM:PET mass ratio of 1.0:0.3. The as-obtained product under the optimal conditions was denoted as Sample SP in the following studies. Furthermore, Fig. 3 demonstrated the element distribution of Sample SP by TEM elemental mapping, with the observation of both plate-like polygonal particles and granular ones (Fig. 3a). The polygonal particles, with a typical diameter of ~200 nm, were concentrated by Mn and O coincidently, which confirmed the formation of MnO as detected by XRD technique. The granular particles were much smaller in diameter (~ 100 nm), with only Ni and Co distributed uniformly, indicating the formation of Ni and Co solid solutions.

Degradation behavior of PET via synergetic pyrolysis

The mass losses with the elevated temperatures were analyzed to understand the thermal behavior of the blended NCM-PET system. As shown in Fig. 4a, the synergetic pyrolysis displayed a three-stage process, when pyrolysis temperature was gradually increased from room temperature to 1000°C. To be specific, stage 1 took place between 310-549°C, in which the mass dropped rapidly by 32.8% and the peak rate of mass loss occurred at 429°C. Stage 2 was relatively prolonged and tardily with 14.0% of total mass lost from 549 to 643°C, including two peaks of mass loss rate at 589°C and 623°C. Stage 3 could lead to a mass loss of 5.3% at 643-840°C with a typical peak located at 713°C. The mass change persisted with a very low rate after the temperature exceeding

840°C. The volatile compounds released during pyrolysis were simultaneously monitored by combining FT-IR and MS measurements. The chemical structure of volatile products was revealed in the 3D FT-IR spectrum, as shown in Fig. 4b. To precisely identify the released gaseous species, , the mass information of each evolved specie and its ion current was detected by the MS (Fig. 4c-4m) measurement.

The peaks collected in 3D FT-IR spectrum indicated the release of various types of volatile compounds, including hydrocarbons (saturated, unsaturated and aromatic hydrocarbons), aldehydes, carboxyls, carbon oxides, and water. The formation of hydrocarbons was confirmed with the peak located at around 1380 cm^{-1} (the bending vibration of C-H bond) of the FT-IR spectra. The specific species were identified as CH_4, $C_2H\cdot$, $C_4H_3\cdot$ and $C_5H_5\cdot$ corresponding to the ion curves of m/z = 15, 25, 51, and 65 in Fig. 4c, 4e, 4k, and 4l, respectively. Among them, the CH_4 and $C_2H\cdot$ were released at Stage 1, while the $C_4H_3\cdot$ and $C_5H_5\cdot$ were mainly generated at Stage 2. Benzene was also observed as reflected in the single ion curve of m/z = 78 (Fig. 4m), and it was released at both Stage 1 and the early period of Stage 2 (before 600°C). In addition to hydrocarbons, the formation of aldehyde groups was also suggested by the FT-IR results. The strong absorbance peak at around 1750 cm^{-1} was ascribed to the stretching vibration of C=O and the peak at 2820 cm^{-1} was attributed to the C-H stretching vibration in the aldehyde[24]. The ion curves of m/z = 29 (Fig. 4g) and 43 (Fig. 4h) were regarded as formyl radical and acetaldehyde, respectively. This indicated that the majority of these two aldehydes was evolved at Stage 1, while a small amount of formyl

radicals was produced at Stage 2. Furthermore, the weak peaks at 3735-3580 cm^{-1} and 1084 cm^{-1} were correspondingly attributed to the vibration of O-H bond and stretching vibration of C-O bond, respectively, corresponding to the bending mode of ester and carboxylic acid. Thus, the m/z = 45 ion curve (Fig. 4j) could be identified as carboxyl acid radicals, according to the PET degradation behavior[22] throughout Stage 1, 2 and 3 until 800°C. In addition, the intense peaks at 2439 cm^{-1} of the FT-IR spectra were the asymmetrical stretching vibration of C=O, which should be related to the formation of CO and CO_2 in ion curves with m/z = 28 (Fig. 4f) and 44 (Fig. 4i). Obviously, CO was mainly produced at Stage 1 and 2, while the CO_2 was gradually released at all three stages. Besides, the absorbance peaks at 1510 and 3739 cm^{-1} were coincident with the ion curve of m/z = 18, which represented that most of H_2O was also produced at the first two stages.

To summarize, PET plastics in the NCM blended system was mainly degraded at three reaction stages and the amount of the released gaseous products, including hydrocarbon (alkane, alkene, alkyne and benzene), aldehyde, carboxylic acid, CO_2, CO and H_2O, was gradually weakened from Stage 1 to Stage 3. According to previous studies[22,24,25,36,37], pure PET displayed a single but rapid degradation stage at 400-500°C with the maximum degradation rate over 400°C. The pyrolysis of pure PET began with the break of ester links, which caused chain scission and produced carboxylic acid and olefinic at the end of chains. Subsequently, the disintegration and secondary reactions continued till the end of degradation mainly by the repeated decarboxylation and free

radical reactions. Thus, the decarboxylation and free radical reactions were the most pivotal and dominant mechanism for pure PET pyrolysis and were also considered as crucial step in synergetic pyrolysis of this study. As a comparison, the degradation of PET with NCM in this study was initiated at a similar temperature (400°C), but the completion of degradation was delayed to Stage 3 at over 800°C. Furthermore, similar gaseous species were detected in the PET-NCM system, when compared with the pure PET system. This indicated the similar degradation pathways in these two systems. For instance, the carboxylic acid was released throughout the three stages, indicating that the decarboxylation reaction was one of the dominate reactions during synergetic pyrolysis. Among other volatile organic compounds, the system produced organic molecules with shorter C-chain (1-2 C atoms) at Stage 1, and then, benzene and larger molecules (4-6 C atoms) were generated mainly at Stage 2. This should be explained by the continuous chain scission and free radical reactions after ester scission. In the residual chain of PET, the carbons at the ends (and adjacent atoms) were more likely to escape, due to the reaction with free radicals, thus generating smaller molecules with 1-2 C atoms. Afterwards, the benzene ring, which was originally located at the middle of the chain, was exposed to the end and thus reacted, generating larger molecules with 4-6 C atoms. In addition, the formation of alkenes and alkynes was possibly resulted from reduction reactions caused by free radicals. Therefore, the decarboxylation and free radical reaction played an essential role in NCM-PET pyrolysis as well. The produced free radicals and reducing gases (e.g., CO and CO_2) not only contributed to

the pyrolysis of PET, but also played key roles in the decomposition and reduction of NCM.

Reaction mechanisms

The DFT calculation was applied to optimize the models and investigate the binding energies between PET and NCM molecules. The polar (001) surface was reported with low surface energy and large surface area, according to previous studies, and thus was chosen as the slab model surface[38,39]. The variables of different adsorption configurations can be described as follows. The Li, TM and O were served as terminations of NCM (001) slab, while the vertical and horizontal planes of the benzene ring were possible adsorption postures of PET. The O, C and H were adsorption sites on PET. After optimization, the binding energies of each adsorption configuration were summarized in Table 1, while a lower adsorption energy represented an easier generation of a more stable configuration. The exact configurations for each model were demonstrated in Fig. S2-S5 of SI.

For the PET adsorption on the Li surface, more Li-O bonds were formed with lower adsorption energies, when the PET was in horizontal position. Configurations 1, 2 and 3 were similar in both configuration type and adsorption energy after optimization (Fig. S2 of SI), implying that the O atoms in ester and carboxyl groups were likely to form single bonds with 1-3 Li atoms on the surface of NCM (001) slab. As the plane of four

O was parallel to Li surface, due to lying benzene, the 6-8 Li-O bonds were generated for each PET model and the lowest adsorption energy was -4.248 eV. The O (Configuration 4) and H (Configuration 5) in vertical PET were found combinative to Li surface as well, but the combination was much weaker because of the higher adsorption energy. The PET adsorption on the TM surface also showed preference in horizontal position, but with a weaker combination (adsorption energy as -2.760 eV) than that on the Li surface. For horizontal PET (Configuration 6), 2 O and 2 C atoms in the PET were adsorbable to the TM surface, forming 4 O/C-TM bonds. Vertical PET allowed only single O-TM or H-TM bond in each configuration (Configurations 7-10) with very weak combination especially regarding H-TM combination. The interaction between PET and O surface was negligible with the adsorption energy closing to 0. In general, PET showed an evident bonding preference on Li over TM and O. Moreover, horizontal PET tended to be adsorbed more easily, compared with the vertical one. This should be attributed to the simultaneous multiple bonding allowed by the planar distribution of atoms on and around the benzene rings. In addition, the O served as the most active atom in PET and provided stronger bonds to NCM (Li and TM), in comparison with the C and H atoms.

Taking all the findings into consideration, the synergetic behavior of the PET-NCM pyrolysis could be comprehensively discussed. On one side, the decomposition of NCM was evidently accelerated, that is, the starting temperature of the thermal decomposition was significantly dropped to 400°C and the effective Li-TM separation was completely

finished at only 550°C. On the other side, the degradation of PET was prolonged to stages of higher temperatures. The changes in thermal behaviors of NCM and PET were in agreement with the coupling reaction mechanisms, consistent with previous studies. This phenomenon implied that a low-temperature reaction could reduce the energy barrier of a high-temperature one[18,24]. The reasons of the coupling effect could be explained as below. First, the early decomposition of NCM was caused by the surface adsorption of PET on the NCM. However, as shown in Fig. 6, pure NCM possessed high thermal stability and remained non-reactive even at 800°C. With the addition of PET in the reaction system, the O atoms in the PET were adsorbable to metal atoms in the NCM, and the capture on Li was stronger than that on TM. In the crystals of NCM, the Li atoms were connected to the lattice by ionic bonds, which were much more fragile and easily broken compared with the covalent bonds of the TM. As a result, the Li-O bonding during the reaction processes extracted Li from the NCM and captured O together with the neighboring C from the PET, leading to the formation of Li_2CO_3. Meanwhile, the TM and O remained in the octahedron framework of the NCM and formed metal oxides, which might be more active owing to the partially collapsed lattice structure. As a support of Li escape and lattice collapse, the XRD patterns in Fig. 1a confirmed the formation of Li_2CO_3, MnO and $Ni_xCo_{1-x}O$ at 550°C and the formation of Ni_xCo_{1-x} at higher temperatures. Second, the pyrolysis of PET released various free radicals and reductive gaseous products, including carboxylic acid, CO, CO_2, CH_4, etc. Previous studies revealed that the reducing gases were more attractive to the O atoms and caused the continuous O escaping and bond breaking in NCM[18,40]. The

indispensable role of the PET on the stepwise reduction of TM was well proved by the transformation from $Ni_xCo_{1-x}O$ to Ni_xCo_{1-x} with the PET increasing from 1.0:0.2 to 1.0:0.3 (Fig. 1c).

Metal recovery and NCM regeneration

Fig. 5a showed the recycling process for NCM recycling with synergetic pyrolysis of PET plastics. After synergetic pyrolysis, water washing was adopted for effective separation of Li from TM, because the soluble Li_2CO_3 can be easily extracted from the solid phase (Sample SP). By means of a simple filtration process, the Li_2CO_3 could be concentrated in the leachate and was crystalized after drying (Sample P-Li). Meanwhile, the insoluble particles in the solid phase (Sample P-TM) were mainly composed of metal oxides, elemental transition metals and PET-derived carbon. As expected, the typical XRD patterns in Fig. 5b verified a successful Li-TM separation. It is obvious that Li_2CO_3 was formed in the Sample P-Li with simultaneous formation of MnO and Ni_xCo_{1-x} in Sample P-TM. The XRD results also suggested that water washing could successfully separate Li_2CO_3 from the TM phases, based on the difference in solubility. The recovery rate of each element was further illustrated in Fig. 5c, which implied that more than 99% of Li was recovered in Sample P-Li and over 99% of Ni, Co and Mn could be recycled in Sample P-TM. Besides, Ni, Co and Mn were not detectable in Sample P-Li and no Li was found in Sample P-TM, thus revealing that water washing could achieve high efficiency and selectivity for the separation of Li and TM. The as-

obtained Sample P-Li and P-TM, possessing high metal purity, could be potentially used as feedstocks for practical applications.

In this work, Sample P-Li and P-TM, viewed as potential battery raw materials, were employed to regenerate NCM cathode materials. By solid-state sintering, the following reactions (eqs. 4 & 5) were expected to take place, inducing the crystallization of new NCM from Li and TM precursors and the calcination of organic compounds with the participation of oxygen. Thus, the sintering step regenerated NCM and removed residual carbon simultaneously.

$$6\,Li_2CO_3 + 4\,Ni + 4\,Co + 4\,MnO + 7O_2 \rightarrow\ 12\,LiNi_{1/3}Co_{1/3}Mn_{1/3}O_2 + 6\,CO_2 \quad (4)$$

$$4\,C_xH_yO_z + (4\mathrm{x} + \mathrm{y} - 2\mathrm{z})O_2 \rightarrow 4\mathrm{x}\,CO_2 + 2\mathrm{y}\,H_2O \quad (5)$$

As evidenced in Fig. 5b, the XRD pattern of the regenerated NCM showed that NCM crystal phase of high purity was observed with sharp peaks, which are corresponding to the α-$NaFeO_2$ structure. This confirmed that the regenerated NCM could be well crystallized with the above solid-state sintering method. Meanwhile, no peaks of other crystal phases were observed, suggesting a complete participation of Li/TM feedstocks and phase transformation to NCM. The doublet peaks of (008)/(110) and (006)/(102) split clearly and sharply, which was considered as crucial indicator for the layer structure in NCM cathode materials[41,42]. The morphology and microstructure of the

regenerated NCM materials were further characterized by SEM and HR-TEM. Fig. 5d showed the micro-scale spherical particle was agglomerated by regular nano-scale polyhydron particles with a typical size of 200-800 nm. The morphology was similar to previous studies on NCM cathode materials, which revealed the restoration of the crystal structure[43,44,45]. Previous studies also reported that small particle size and uniform distribution were beneficial for the cycling and C-rate performances of NCM, and certain agglomeration could enhance electrochemical charge-discharge performance, owing to better ionic conductivity provided by the inter-connection between particles[46]. HR-TEM image in Fig. 5e showed two sets of clear fringes, and the inter planar spacing was observed as 0.48 nm and 0.24 nm, assigned to the (003) and (101) planes of NCM, respectively. The FFT (fast Fourier transform) pattern revealed that the particle was preferentially exposed with (003) plane, which was consistent with the above XRD results, thus verifying a typical (003) crystal plane of the layered phase in the regenerated NCM cathode materials.

Discussion

Until most recently, many studies have focused on recycling spent cathode materials via pyrolysis strategy, and some of them need to reply on additional chemicals to overcome critical technical challenges, such as high energy consumption, low lithium recovery rate and secondary pollution, etc. The carbon-contained reductants were chosen as one of the environmentally friendly reducing agents for pyrolysis process.

However， high reaction temperatures are still required for achieving high recovery rate of metal elements. To achieve economic feasibility, it is highly desirable to develop energy saving process for pyrolysis recycling of battery materials. It is well known that PET is one of the most widely used polymers for disposable plastic products, which contributed to a tremendous volume of waste generation, thus leading to serious environmental concerns. PET can be decomposed into fuel sources by catalytic reactions, with simultaneous generation of large amounts of free radicals and gases, which could greatly reduce the pyrolysis temperature for the thermal decomposition of the other co-pyrolyzation substances. Inspired by this phenomenon, this study proposed a facile synergetic pyrolysis strategy for NCM-PET system, which was highly efficient for element recovery and beneficial to both economy and environment.

The results of this study suggested that the synergetic pyrolysis system could greatly reduce the decomposition temperature of NCM to 550°C with the simultaneous generation of Li_2CO_3, $Ni_xCo_{1-x}O$, Ni_xCo_{1-x} and MnO as the product phases. Meanwhile, the PET addition of 1.0:0.3 (NCM/PET mass ratio) was enough to complete the decomposition reaction within only 30 min. The results in this work were further compared with previous studies, as shown in Table S2 of SI. For instance, when coke, graphite or carbon were used as reductants, the pyrolysis temperatures were typically in the range of 650-1000°C, with a duration time of 60-180 min. Meanwhile, the complete decomposition of NCM was achieved with only 550°C, much lower than previous work. In addition, owing to relatively low pyrolysis temperature, high

retention of the valuable metal elements (over 99%) in the pyrolyzed products was confirmed, especially for the volatile Li element. This energy saving strategy was potentially applicable for efficient recovery of valuable metals (e.g. Li, Ni, Co and Mn) from spent LIBs through simple post treatment (e.g. water washing). It should be emphasized that disposal and resource utilization of the plastic waste was demonstrated for battery recycling technology. Thereafter, a simple but efficient water washing step could successfully separate Li and TM with high recovery rate (over 99%) and high purity (no impurity metals detected). In addition, new NCM material with well layered structure was successfully regenerated by sintering the recovered Li- and TM-precursors at 800°C, and the residual carbon was simultaneously decomposed under air atmosphere. It should be mentioned that more detailed physicochemical properties and electrochemical performances of the regenerated NCM materials will be reported in the future work. Furthermore, the exploration of reaction mechanisms provided theoretical basis for industrial applications and migration applications. Overall, this study provided a thinking of using plastic properties to achieve a win-win situation by simultaneous treatment of plastic waste and battery wastes for valuable metal recovery.

Methods

Materials and reagents

Battery grade $LiNi_{1/3}Co_{1/3}Mn_{1/3}O_2$ (NCM333) powder sample received from Shenzhen Kejing Zhida Technology Co., Ltd. was used in this work, instead of spent cathode materials. PET sample was received from Qingdao Usolf Chemical Technology Co., Ltd. Note that no other chemicals or reagents were employed in the pyrolysis and post-treatment processes. For metal element quantification, HCl (37 wt%), HNO_3 and H_2O_2 (30 wt%) (volume ratio 9:3:1) of analytical grade were purchased from Shanghai Aladdin Bio-Chem Technology Co., Ltd., and used as the digestion solution.

Synergetic pyrolysis and sample characterization

The effects of three key factors, including temperature, NCM:PET mass ratio and dwelling time on crystal phase change were systematically investigated in this study. The dried NCM and PET powder were mixed via ball-milling (QM-QX-2L, MITR) at 3000 rpm for 30 min. The effect of PET addition on crystal phase change was studied using six gradients of NCM:PET mass ratio (1.0:0.1, 1.0:0.2, 1.0:0.3, 1.0:0.4, 1.0:0.5, and 1.0:1.0). The sample mixture was then added into a quartz crucible and placed in a tube furnace (OTF-1200X-II-100, Kejing., China) for synergetic pyrolysis. The pyrolysis was conducted under N_2 atmosphere with a flow rate of 0.3 L min^{-1}, and a heating rate of 10°C min^{-1}. To individually explore the effect of pyrolysis temperature, the mixture was heated at different target temperatures (400, 500, 550, 600, 700, 800, 900, and 1000°C) for a fixed time (120 min), and the effect of dwelling time on crystal

phase change was investigated by heating at a fixed temperature (400°C) for different dwelling time (15, 30, 60, 90, and 120 min).

X-ray diffraction (XRD, Rigaku SmartLab) technique was applied to identify the phase transformation behavior during the pyrolysis, and the XRD patterns were recorded under monochromated Cu $K_{\alpha 1}$ radiation operating at 45 kV and 200 mA from 10 to 90° (10° min^{-1}). To determine the content of metals in the pyrolyzed products, the solid products were digested with acids and metal elements (Li, Co, Ni, and Mn) were quantified by inductively coupled plasma-optical emission spectrometry (ICP-OES; 8000 Perkin Elmer). The morphology and element distribution of the products were obtained by the scanning transmission electron microscopy - energy dispersive X-ray (STEM-EDX) by a Tecnai G2 F30 (Thermo Fisher) microscope operating at an accelerating voltage of 300 kV. The mass change of all pyrolysis samples was recorded to calculate the loss of ignition (LOI).

In particular, the thermal behavior of the blended NCM/PET system, especially regarding evolutionary components, was monitored using a thermogravimetric analysis (TGA, 209F1, NETZSCH) coupled with a mass spectroscopy (MS, QMS403C, NETZSCH) and a Fourier transform infrared spectroscopy (FT-IR, Nicolette-IS-50, Thermo Fisher) separately. Typically, 30 mg of the NCM-PET mixture with a mass ratio of 1.0:1.0 was loaded in an alumina crucible, and the thermal behavior was monitored from 30 to 1000°C under N_2 atmosphere with a heating rate of 10°C min^{-1}.

Post-treatment and sample characterization

The products obtained under the optimal pyrolysis condition (marked as Sample SP) was washed with the deionized water at room temperature to separate Li and TM elements. Sample SP was added into the deionized water with a solid/liquid ratio of 20 g/L, and then the mixture was treated with a shaker (TS-212N, TENSUC) at 100 rpm for 60 min. [16,30,31] After simple washing, the solid residue (denoted as Sample P-TM) was filtered and separated from the leachate. The leachate was then evaporated under 90°C to obtain another solid product (Sample P-Li). The supposed Li- and TM-concentrated products were denoted as Sample P-Li and P-TM, respectively.

The content of all metal elements in the post-treatment products was quantified by ICP-OES after acid digestion, to determine the purity of the product and the metal recovery rate of the progress. The recovery rate of the targeted metal elements in the recovered products was calculated with the below equation (1):

$$R_i = \frac{m_P \cdot wt\%_{iP}}{m_R \cdot wt\%_{iR}} \times 100\% \quad (1)$$

where $wt\%_{iP}$ and $wt\%_{iR}$ are the weight content of metal "i" in the recovered product (P, referring to Sample P-Li or P-TM) and the raw NCM-PET mixture (R), respectively; m_P and m_R are the weight of recovered product and raw mixture, respectively.

The weight content was calculated as equation (2):

$$wt\%_i = \frac{c_i \cdot V}{m} \times 100\% \quad (2)$$

where c_i, V and m are the concentration of metal i in the digested solution, the volume of the digested solution and the mass of the digested sample, respectively.

The new NCM was then resynthesized by using the recovered Sample P-Li and P-TM in previous steps. After confirming the content of Li in Sample P-Li and the content of Ni, Co and Mn in Sample P-TM, the two solid samples were weighed to reach the molar ratio of Li:TM (Ni + Co + Mn) = 1.1:1.0 and then fully mixed by ball-milling at 3000 rpm for 30 min. The as-obtained solid mixture was then transferred to a muffle furnace (KSL-1200X-M, Kejing., China) and sintered at 800°C for 10 h with a ramping rate of 5°C min^{-1} under air atmosphere, resulting in the regenerated NCM (Sample R-NCM). XRD was applied to identify the crystal phases in the solid products. Scanning electron microscope (SEM) was performed to observe the sample morphology on a FEI Nova NanoSem 450. High resolution TEM (HR-TEM) data was collected to characterize the microscopy in nano-scales.

DFT calculation

Density functional theory (DFT) calculation was carried out to harvest the adsorption preference of NCM and PET particles. Spin-polarized DFT calculations were performed using the Vienna ab initio simulation package (VASP)[32,33]. The generalized gradient approximation proposed by Perdew, Burke, and Ernzerhof (GGA-PBE) was selected for the exchange-correlation potential[34]. The pseudo-potential was described by the projector-augmented-wave (PAW) method[35]. The geometry optimization was performed until the Hellmann–Feynman force on each atom was smaller than 0.02 eV/Å. The energy criterion was set to 10^{-6} eV in iterative solution of the Kohn-Sham equation. The NCM (001) slab model was constructed by cleaving the (001) surface of LCO unit cell and expanding into a 4a*5b*c supercell, and the Co atoms were randomly replaced by 1/3 Ni and 1/3 Mn atoms. Li, TM, or O terminations on the slab model surface were investigated and compared. 18 Å vacuum above the slab model was created. During optimization, only the top three layers of atoms were allowed to relax. The adsorption energy (E_{ads}) was calculated according to equation (3)

$$E_{ads} = E_{total} - E_1 - E_2 \quad (3)$$

in which E_{total} is the DFT energy of NCM (001) with PET adsorbed, E_1 is NCM (001) energy and E_2 is PET energy.

Data availability

The data that support the findings of this study are available from the corresponding author upon reasonable request.

Acknowledgements

The authors are grateful to the National Natural Science Foundation of China (42277403; 41977329), and the Natural Science Foundation of Guangdong Province (2021B1515020041) for financial support. Also, we want to thank the State Environmental Protection Key Laboratory of Integrated Surface Water-Groundwater Pollution Control, Center for Computational Science and Engineering at Southern University of Science and Technology (SUSTech), and core research facilities at SUSTech to provide quality resources and services. Dr. Xiao-ying Lu would like to thank the financial support from Hong Kong Environment and Conservation Fund (No.: 39/2019) and Hong Kong Competitive Research Funding Schemes for the Local Self-financing Degree Sector Faculty Development Scheme (No.: UGC/FDS25/E06/19).

Supporting Information

The supporting information is available, including 2 Tables and 5 Figures.

References

1. Makuza, B., Tian, Q., Guo, X., Chattopadhyay, K. & Yu, D. Pyrometallurgical options for recycling spent lithium-ion batteries: A comprehensive review. *Journal of Power Sources* **491**

(2021).

2. Miao, Y., Liu, L., Zhang, Y., Tan, Q. & Li, J. An overview of global power lithium-ion batteries and associated critical metal recycling. *J Hazard Mater* **425**, 127900 (2022).
3. Makuza, B., Yu, D., Huang, Z., Tian, Q. & Guo, X. Dry Grinding - Carbonated Ultrasound-Assisted Water Leaching of Carbothermally Reduced Lithium-Ion Battery Black Mass Towards Enhanced Selective Extraction of Lithium and Recovery of High-Value Metals. *Resources, Conservation and Recycling* **174** (2021).
4. Yu, Z., Lu, F., Zou, Y. & Yang, X. Quantifying energy flexibility of commuter plug-in electric vehicles within a residence–office coupling virtual microgrid. Part II: Case study setup for scenario and sensitivity analysis. *Energy and Buildings* **254** (2022).
5. Harper, G., Sommerville, R., Kendrick, E. *et al.* Recycling lithium-ion batteries from electric vehicles. *Nature* **575**, 75–86 (2019).
6. R.A. Market https://www.researchandmarkets.com/reports/4805605/li-ion-battery-global-market-trajectory-and#rela3–5021667 (access date: Dec 2022)
7. Xiao, J., Guo, J., Zhan, L. & Xu, Z. A cleaner approach to the discharge process of spent lithium ion batteries in different solutions. *Journal of Cleaner Production* **255** (2020).
8. Velázquez, M., Valio, Santasalo, A., Reuter & Serna, G. A Critical Review of Lithium-Ion Battery Recycling Processes from a Circular Economy Perspective. *Batteries* **5** (2019).
9. Chen, Y. *et al.* Thermal treatment and ammoniacal leaching for the recovery of valuable metals from spent lithium-ion batteries. *Waste Manag* **75**, 469-476 (2018).
10. Ren, J. *et al.* The impact of aluminum impurity on the regenerated lithium nickel cobalt manganese oxide cathode materials from spent LIBs. *New Journal of Chemistry* **41**, 10959-

10965 (2017).

11. Fan, E. *et al.* Low-Temperature Molten-Salt-Assisted Recovery of Valuable Metals from Spent Lithium-Ion Batteries. *ACS Sustainable Chemistry & Engineering* **7**, 16144-16150 (2019).
12. Peng, C., Liu, F., Wang, Z., Wilson, B. P. & Lundström, M. Selective extraction of lithium (Li) and preparation of battery grade lithium carbonate (Li_2CO_3) from spent Li-ion batteries in nitrate system. *Journal of Power Sources* **415**, 179-188 (2019).
13. Lin, J. *et al.* Environmentally benign process for selective recovery of valuable metals from spent lithium-ion batteries by using conventional sulfation roasting. *Green Chemistry* **21**, 5904-5913 (2019).
14. Lin, J. *et al.* Conversion Mechanisms of Selective Extraction of Lithium from Spent Lithium-Ion Batteries by Sulfation Roasting. *ACS Appl Mater Interfaces* **12**, 18482-18489 (2020).
15. Di, C. *et al.* in *Energy Technology 2020: Recycling, Carbon Dioxide Management, and Other Technologies The Minerals, Metals & Materials Series* Ch. Chapter 37, 387-395 (2020).
16. Tang, Y. *et al.* Recovery and regeneration of $LiCoO_2$-based spent lithium-ion batteries by a carbothermic reduction vacuum pyrolysis approach: Controlling the recovery of CoO or Co. *Waste Manag* **97**, 140-148 (2019).
17. Liu, C., Lin, J., Cao, H., Zhang, Y. & Sun, Z. Recycling of spent lithium-ion batteries in view of lithium recovery: A critical review. *Journal of Cleaner Production* **228**, 801-813 (2019).
18. Zhao, Y. *et al.* Regeneration and reutilization of cathode materials from spent lithium-ion batteries. *Chemical Engineering Journal* **383** (2020).
19. Zhang, B. *et al.* A sodium salt-assisted roasting approach followed by leaching for recovering spent $LiFePO_4$ batteries. *J Hazard Mater* **424**, 127586 (2022).

20. Zhou, F. *et al.* Vacuum Pyrolysis of Pine Sawdust to Recover Spent Lithium Ion Batteries: The Synergistic Effect of Carbothermic Reduction and Pyrolysis Gas Reduction. *ACS Sustainable Chemistry & Engineering* **10**, 1287-1297 (2022).

21. Lan Tiseo. Market volume of polyethylene terephthalate worldwide from 2015 to 2021, with a forecast for 2022 to 2029. https://www.statista.com/statistics/1245264/polyethylene-terephthalate-market-volume-worldwide/

22. Çit, İ. *et al.* Comparative pyrolysis of polyolefins (PP and LDPE) and PET. *Polymer Bulletin* **64**, 817-834 (2009).

23. Dimitrov, N., Kratofil Krehula, L., Ptiček Siročić, A. & Hrnjak-Murgić, Z. Analysis of recycled PET bottles products by pyrolysis-gas chromatography. *Polymer Degradation and Stability* **98**, 972-979 (2013).

24. Singh, R. K., Ruj, B., Sadhukhan, A. K. & Gupta, P. A TG-FTIR investigation on the co-pyrolysis of the waste HDPE, PP, PS and PET under high heating conditions. *Journal of the Energy Institute* **93**, 1020-1035 (2020).

25. Xu, J. *et al.* Compatibilization of Isotactic Polypropylene (iPP) and High-Density Polyethylene (HDPE) with iPP–PE Multiblock Copolymers. *Macromolecules* **51**, 8585-8596 (2018).

26. Chakraborty, A., Kunnikuruvan, S., Dixit, M. & Major, D. T. Review of Computational Studies of NCM Cathode Materials for Li-ion Batteries. *Israel Journal of Chemistry* **60**, 850-862 (2020).

27. Kramer, D. & Ceder, G. Tailoring the Morphology of $LiCoO_2$: A First Principles Study. *Chemistry of Materials* **21**, 3799-3809 (2009).

28. Guo, Y. *et al.* Efficient degradation of industrial pollutants with sulfur (IV) mediated by $LiCoO_2$ cathode powders of spent lithium ion batteries: A "treating waste with waste" strategy. *J Hazard*

Mater **399**, 123090 (2020).

29. Özsin, G. & Pütün, A. E. TGA/MS/FT-IR study for kinetic evaluation and evolved gas analysis of a biomass/PVC co-pyrolysis process. *Energy conversion and management* **182**, 143-153 (2019).
30. Hu, J., Zhang, J., Li, H., Chen, Y. & Wang, C. A promising approach for the recovery of high value-added metals from spent lithium-ion batteries. *Journal of Power Sources* **351**, 192-199 (2017).
31. Hekmatfar, M., Kazzazi, A., Eshetu, G. G., Hasa, I. & Passerini, S. Understanding the Electrode/Electrolyte Interface Layer on the Li-Rich Nickel Manganese Cobalt Layered Oxide Cathode by XPS. *ACS Appl Mater Interfaces* **11**, 43166-43179 (2019).
32. Kresse, G. & Comput. Efficiency of ab-initio total energy calculations for metals and semiconductors using a plane-wave basis set. *Computational Material Science*, **6**, 15-50 (1996).
33. Kresse, G. & Furthmüller, J. Efficient iterative schemes for ab initio total-energy calculations using a plane-wave basis set. *Physical Review B*, **54**, 11169 (1996).
34. Perdew, J. P., Burke, K. & Ernzerhof, M. Generalized gradient approximation made simple. *Physical Review Letters*, **77**, 3865 (1996).
35. Blöchl, P. E. Projected augmented-wave method. *Physical Review B*, **50**,17953 (1996)
36. Honus, S., Kumagai, S., Fedorko, G., Molnár, V. & Yoshioka, T. Pyrolysis gases produced from individual and mixed PE, PP, PS, PVC, and PET—Part I: Production and physical properties. *Fuel* **221**, 346-360 (2018).
37. Honus, S., Kumagai, S., Molnár, V., Fedorko, G. & Yoshioka, T. Pyrolysis gases produced from individual and mixed PE, PP, PS, PVC, and PET—Part II: Fuel characteristics. *Fuel* **221**, 361-373 (2018).

38. Hong, L. *et al.* Electronic Structure of $LiCoO_2$ Surfaces and Effect of Al Substitution. *The Journal of Physical Chemistry C* **123**, 8851-8858 (2019).

39. Bennett, J. W., Jones, D., Huang, X., Hamers, R. J. & Mason, S. E. Dissolution of Complex Metal Oxides from First-Principles and Thermodynamics: Cation Removal from the (001) Surface of $Li(Ni_{1/3}Mn_{1/3}Co_{1/3})O_2$. *Environ Sci Technol* **52**, 5792-5802 (2018).

40. Xiao, J., Li, J. & Xu, Z. Novel Approach for in Situ Recovery of Lithium Carbonate from Spent Lithium Ion Batteries Using Vacuum Metallurgy. *Environ Sci Technol* **51**, 11960-11966 (2017).

41. Xi, Y. *et al.* Comparative study of the electrochemical performance of $LiNi_{0.5}Co_{0.2}Mn_{0.3}O_2$ and $LiNi_{0.8}Co_{0.1}Mn_{0.1}O_2$ cathode materials for lithium ion batteries. *Solid State Ionics* **327**, 27-31 (2018).

42. Jiang, T. *et al.* Improved High-Potential Property of Ni-Rich $LiNi_{0.8}Co_{0.1}Mn_{0.1}O_2$ with a Garnet Ceramic LLZTO Surface Modification in Li-Ion Batteries. *ACS Applied Energy Materials* **5**, 305-315 (2021).

43. Li, J., Yao, R. & Cao, C. $LiNi_{1/3}Co_{1/3}Mn_{1/3}O_2$ nanoplates with 010 active planes exposing prepared in polyol medium as a high-performance cathode for Li-ion battery. *ACS Appl Mater Interfaces* **6**, 5075-5082 (2014).

44. Meng, X. *et al.* Recycling of $LiNi_{1/3}Co_{1/3}Mn_{1/3}O_2$ cathode materials from spent lithium-ion batteries using mechanochemical activation and solid-state sintering. *Waste Manag* **84**, 54-63 (2019).

45. Dang, H. *et al.* Lithium leaching via calcium chloride roasting from simulated pyrometallurgical slag of spent lithium ion battery. *Separation and Purification Technology* **233** (2020).

46. Huang, D. *et al.* Nanoscale $LiNi_{0.5}Co_{0.2}Mn_{0.3}O_2$ cathode materials for lithium ion batteries via

a polymer-assisted chemical solution method. *Applied Materials Today* **16**, 342-350 (2019).

Table 1. Information for the optimized adsorption configurations of PET and NCM ($LiNi_{1/3}Co_{1/3}Mn_{1/3}O_2$) (001) slab

No.	Surface of NCM	Posture of PET	Bonding atoms	E_{ad} (eV)
1	Li	horizontal	O-Li	-3.948
2	Li	horizontal	O-Li	-4.248
3	Li	horizontal	O-Li	-4.102
4	Li	vertical	O-Li	-1.080
5	Li	vertical	H-Li	-0.386
6	TM	horizontal	O-TM, C-TM	-2.757
7	TM	vertical	O-TM	-1.328
8	TM	vertical	O-TM	-0.843
9	TM	vertical	O-TM	-1.566
10	TM	vertical	H-TM	-0.832
11	O	horizontal	None	0.076

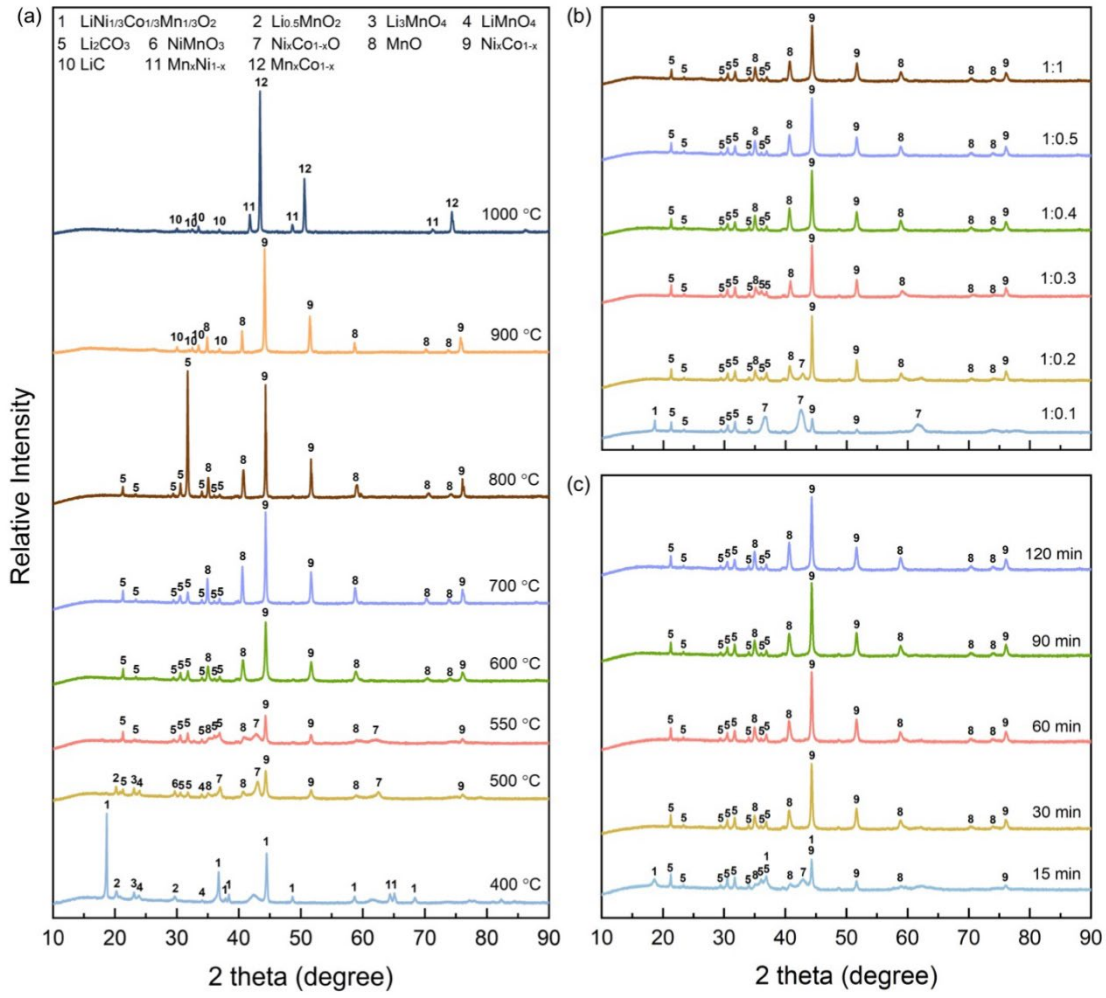

Figure 1 Typical XRD patterns of the PET+NCM ($LiNi_{1/3}Co_{1/3}Mn_{1/3}O_2$) synergetic pyrolysis products (a) at different temperatures (400, 500, 550, 600, 700, 800, 900 and 1000°C) for 120 min, with a mass ratio of NCM/PET of 1.0:1.0, (b) with various mass ratios of NCM/PET (1.0:0.1; 1.0:0.2, 1.0:0.3, 1.0:0.4, 1.0:0.5 and 1.0:1.0) at 600°C for 120 min, and (c) of different time (15, 30, 60, 90 and 120 min) at 600°C, with a mass ratio of NCM/PET of 1.0:0.3.

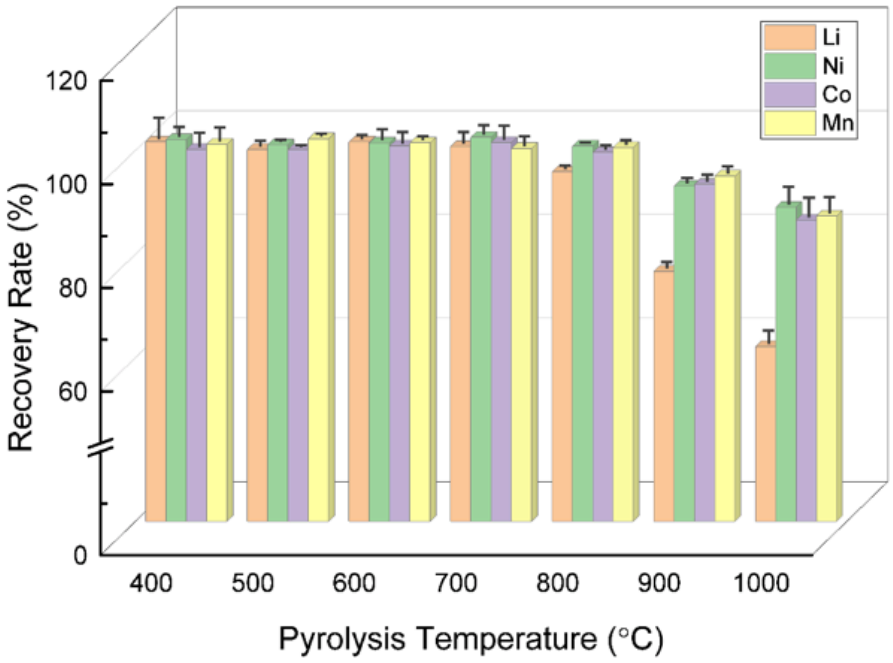

Figure 2 Recovery rate of different metals (Li, Ni, Co and Mn) in the pyrolyzed products obtained at various pyrolysis temperatures.

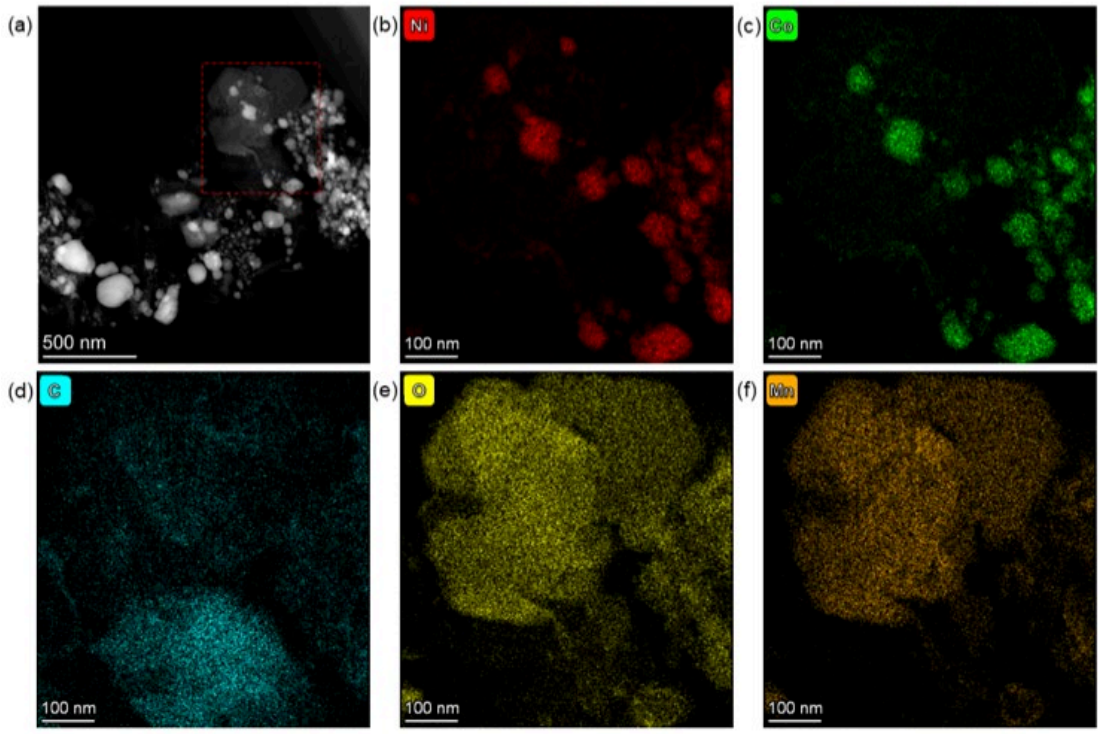

Figure 3 Typical high-resolution EDX mapping of the pyrolyzed products (Sample SP) obtained under pyrolysis conditions of 600°C, 120 min and a NCM ($LiNi_{1/3}Co_{1/3}Mn_{1/3}O_2$)/PET mass ratio of 1.0:1.0.

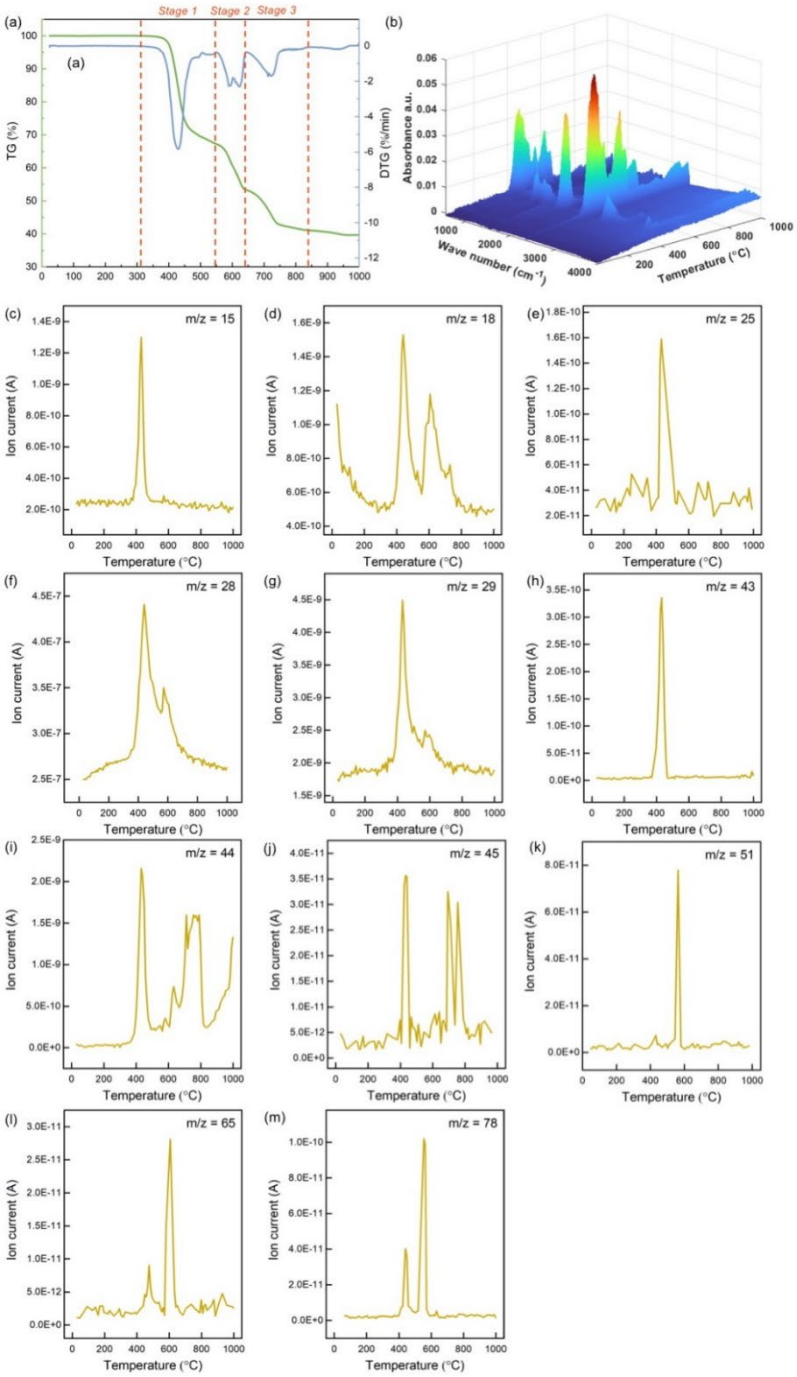

Figure 4 (a) TGA and DTG curves of PET+NCM ($LiNi_{1/3}Co_{1/3}Mn_{1/3}O_2$) mixture from 30 to 1000°C; (b) 3-dimensional FT-IR spectra; and single ion curves in the gas released during TGA analysis, including (c) m/z = 15, (d) m/z = 18, (e) m/z = 25, (f) m/z = 28, (g) m/z = 29, (h) m/z = 43, (i) m/z = 44, (j) m/z = 45, (k) m/z = 51, (l) m/z = 65 and (m) m/z = 78. The loaded mass ratio of NCM/PET was 1.0:1.0.

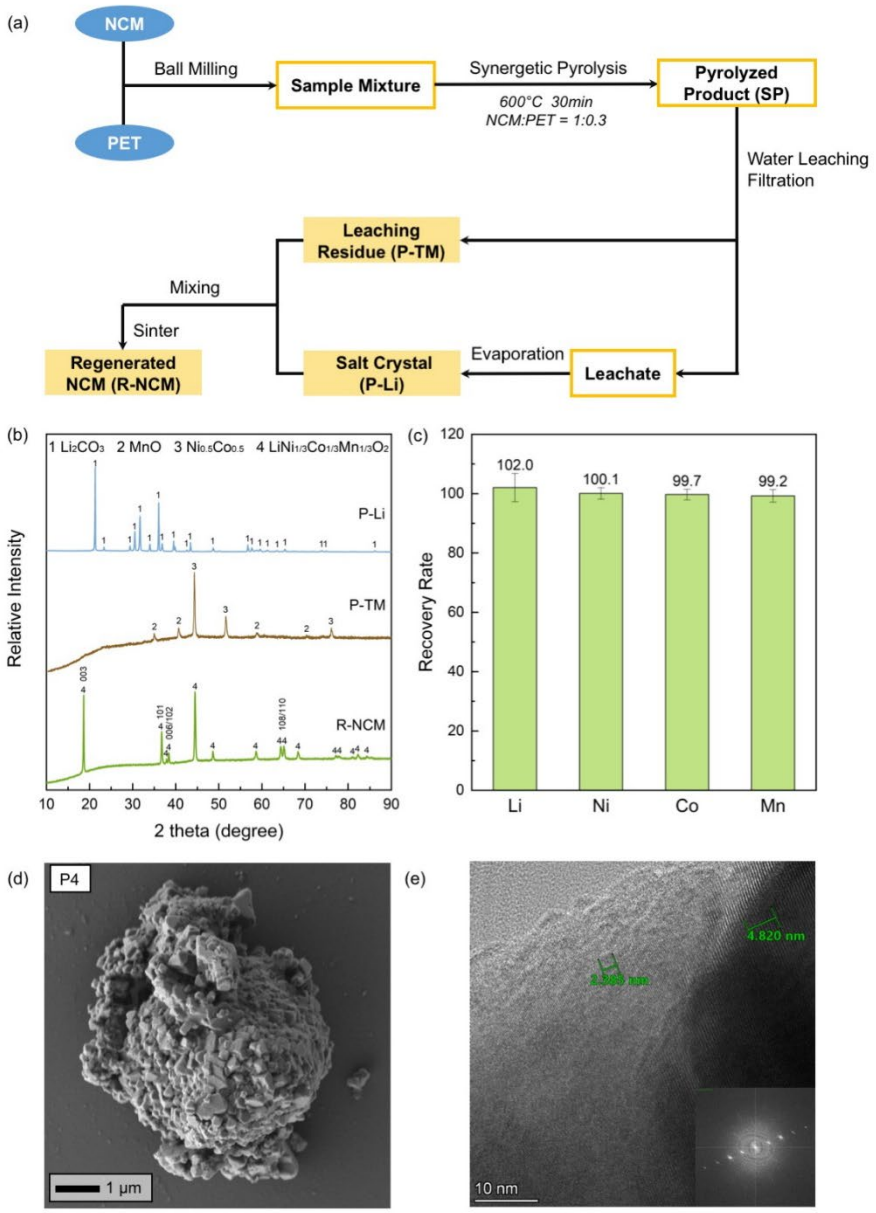

Figure 5 (a) A schematic diagram showing the recycling process of the NCM ($LiNi_{1/3}Co_{1/3}Mn_{1/3}O_2$) powder with synergetic pyrolysis of PET plastics; (b) XRD patterns of the post treatment products, including Sample P-Li, P-TM and R-NCM; (c) content of Li, Ni, Co and Mn in Sample P-Li and P-TM; (d) typical SEM and (e) typical HR-TEM images of Sample R-NCM, including the inset showing the corresponding fast fourier transform (FFT) image.

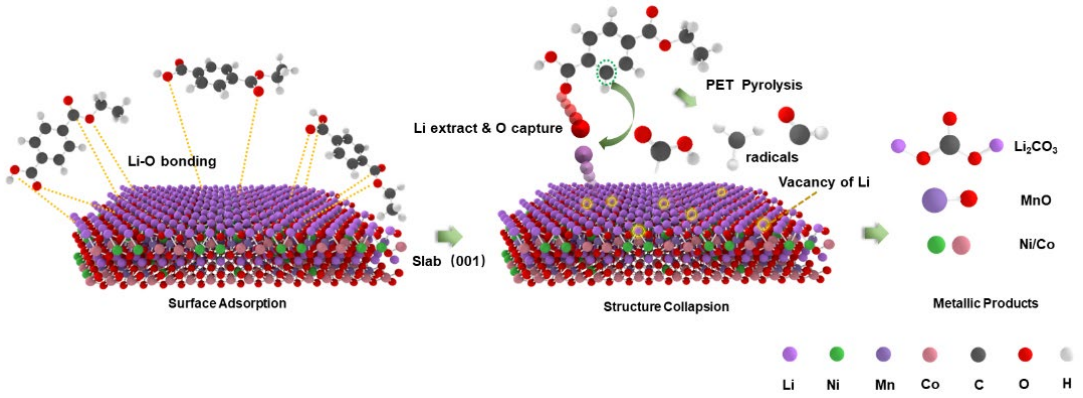

Figure 6. Schematic diagram illustrating the synergetic pyrolysis mechanisms of PET+NCM ($LiNi_{1/3}Co_{1/3}Mn_{1/3}O_2$).